10:02:23 OCA PAD AMENDMENT - PROJECT HEADER INFORMATION 06/17/93

Active

Project #: E-16-M69 Cost share #: Rev #: 1
Center # : 10/24-6-R7690-0A0 Center shr #: OCA file #:
Work type : RES
Contract#: NCA2-761 Mod #: LTR DTD 5/12/93 Document : AGR
Prime #: Contract entity: GTRC

Subprojects ? : N CFDA:
Main project #: PE #:

Project unit: AERO ENGR Unit code: 02.010.110
Project director(s):
PRASAD J V R AERO ENGR (404)894-3043

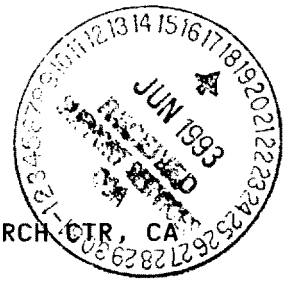

Sponsor/division names: NASA / AMES RESEARCH CTR, CA
Sponsor/division codes: 105 / 006

Award period: 921115 to 930814 (performance) 930831 (reports)

Sponsor amount	New this change	Total to date
Contract value	0.00	26,030.00
Funded	0.00	26,030.00
Cost sharing amount		0.00

Does subcontracting plan apply ?: N

Title: ROTORCRAFT TURBULENCE MODELING AND SIMULATION ABSTRACT

PROJECT ADMINISTRATION DATA

OCA contact: Anita D. Rowland 894-4820

Sponsor technical contact

MR. ADOLPH ATENCIO, JR
(415)604-6863

FLIGHT CONTROLS BRANCH
MAIL STOP 210-7
NASA-AMES RESEARCH CENTER
MOFFETT FIELD, CA 94035-1000

Sponsor issuing office

AMY CHU
(415)604-5238

NASA-AMES UNIVERSITY CONSORTIUM
MAIL STOP 223-9
MOFFETT FIELD, CA 94035-1000

Security class (U,C,S,TS) : U ONR resident rep. is ACO (Y/N): N
Defense priority rating : supplemental sheet
Equipment title vests with: Sponsor GIT
**REF. PG. 1 OF BUDGET, " PURCHASE OF EQUIPMENT IS NOT AN ALLOWABLE COST"
Administrative comments -
NASA LTR DTD 5/12/93 AUTHORIZES AN EXTENSION TO PERIOD OF PERFORMANCE TO 8/14/93, AND FINAL REPORT TO 8/31/93, AS REQUESTED 5/5/93.

GEORGIA INSTITUTE OF TECHNOLOGY
OFFICE OF CONTRACT ADMINISTRATION

NOTICE OF PROJECT CLOSEOUT

Closeout Notice Date 05/03/94

Project No. E-16-M69_____ Center No. 10/24-6-R7690-0A0_

Project Director PRASAD J V R_____ School/Lab AERO ENGR_____

Sponsor NASA/AMES RESEARCH CTR, CA_____

Contract/Grant No. NCA2-761_____ Contract Entity GTRC

Prime Contract No. _____

Title ROTORCRAFT TURBULENCE MODELING AND SIMULATION ABSTRACT_____

Effective Completion Date 930814 (Performance) 930831 (Reports)

Closeout Actions Required:	Y/N	Date Submitted
Final Invoice or Copy of Final Invoice	Y	_____
Final Report of Inventions and/or Subcontracts	Y	_____
Government Property Inventory & Related Certificate	N	_____
Classified Material Certificate	N	_____
Release and Assignment	N	_____
Other _____	N	_____

Comments_____

_____

Subproject Under Main Project No. _____

Continues Project No. _____

Distribution Required:

Project Director	Y
Administrative Network Representative	Y
GTRI Accounting/Grants and Contracts	Y
Procurement/Supply Services	Y
Research Property Managment	Y
Research Security Services	N
Reports Coordinator (OCA)	Y
GTRC	Y
Project File	Y
Other _____	N
_____	N

NOTE: Final Patent Questionnaire sent to PDPI.

ROTORCRAFT TURBULENCE MODELING AND SIMULATION

J.V.R. PRASAD
SCHOOL OF AEROSPACE ENGINEERING
GEORGIA INSTITUTE OF TECHNOLOGY
ATLANTA, GEORGIA 30332

G.H. GAONKAR
DEPARTMENT OF MECHANICAL ENGINEERING
FLORIDA ATLANTIC UNIVERSITY
BOCA RATON, FLORIDA 33431

A. ATENCIO, JR.
FLIGHT CONTROLS BRANCH
NASA AMES RESEARCH CENTER
MOFFETT FIELD, CALIFORNIA

R. MCFARLAND
FLIGHT SIMULATION BRANCH
NASA AMES RESEARCH CENTER
MOFFETT FILED, CALIFORNIA

FINAL REPORT OF WORK PERFORMED
UNDER NASA-UNIVERSITY CONSORTIUM INTERCHANGE
NO. NCA2-761

APRIL 1994

TABLE OF CONTENTS

		Page No.
	SUMMARY	1
1.	INTRODUCTION	2
2.	OBJECTIVES	5
3.	ROTORCRAFT TURBULENCE MODELING	6
4.	ROTORCRAFT TURBULENCE SIMULATION	12
5.	APPROXIMATIONS TO TURBULENCE SIMULATION	15
6.	ROTATIONAL VELOCITY EFFECTS ON BODY RESPONSE	18
7.	CONCLUSIONS	19
8.	RECOMMENDATIONS	20
	REFERENCES	21
	FIGURES	24

LIST OF FIGURES

Figure No.		Page No.
1.	Autospectral densities of fore-to-aft turbulence seen by a rotating blade station and the center of the turbine disk: (1) at the blade station, blade-fixed sampling or with rotational velocity effects; (2) at the turbine disk center, body-fixed sampling or without rotational velocity effects (Ref. 9).	24
2.	Schematic of distance metric ξ.	25
3.	Perspectives of correlation and frequency-time spectrum of turbulence with rotational velocity effects (Rosenbrock model, L/R=4, μ=0.05).	26
4.	Mean square values of flap response (von Karman model, L/R=2, m=0.1).	27
5.	Zero exceedance statistics of flap response (von Karman model, L/R=2, μ=0.1).	28
6.	Sample of simulated helicopter response to two-dimensional turbulence with and without rotational velocity effects (von Karman model, L/R=2, μ=0.1).	29

SUMMARY

This report documents results of rotorcraft turbulence modeling and simulation from a collaborative effort between the Georgia Institute of Technology (Georgia Tech), Florida Atlantic University (FAU) and NASA Ames Research Center. An important outcome of the collaboration is the development of a new simulation method for investigating turbulence effects on rotorcraft. The simulation method takes into account rotational velocity or blade-fixed sampling effects as well as spatial distribution of turbulence velocities over the rotor disk. It is exercised in a comprehensive helicopter flight simulation program to demonstrate qualitatively the blade-fixed sampling effects on vehicle response to turbulence. Various approximations and simplifications to it are also presented, which reduce the computational effort and thereby offer promise to large-dimensional models of comprehensive analysis and real time implementation. The documentation also includes prediction of isolated blade flapping response to turbulence via state-transition and input-covariance matrices and the response statistics agree with the simulation results. An important conclusion is that neglect of blade-fixed sampling effects in modeling and simulation of atmospheric turbulence can lead to erroneous results of turbulence and response statistics.

1. INTRODUCTION

In the presence of turbulence, the flight dynamics requirements of military helicopters are becoming increasingly demanding. Typical examples include nap-of-the-earth maneuvers, near-ground hovering and landing on moving ships with limited accessibility. Turbulence also impacts the flight dynamics of other vehicles which combine the hovering efficiency of the helicopters with the cruising efficiency of airplanes. The tilt rotor "chugging" problem is a case in point, which is basically a fore-to-aft low-frequency acceleration of the rigid body mode coupling with the rotor torque mode. It occurs at relatively low speeds of 150-170 knots and aggravates during descent (Ref. 1). Such developments prompted an improved appreciation of low altitude turbulence modeling, its simulation and its effects on flight dynamics; particularly maneuverability, low-frequency response, stability, pilot's work load, ride quality and flight control system design. In fact, according to a recent NASA/Army study (Ref. 2), the lack of an adequate low-altitude turbulence model is a critical gap in assessing helicopter flight dynamics characteristics. This is well corroborated by comments from pilots "flying" flight simulators. The consequence is that the state-of-the-art rotorcraft simulators include turbulence models only in a rudimentary way in that these models developed for airplanes completely neglect the rotating and translating environment of the rotorcraft. As a result, real-world scenarios are not generally well simulated; worse still, pilots feel that some of the most severe cases cannot be duplicated at all (Ref. 3). Given this background and to put the present study in perspective, three important issues of turbulence modeling and simulation are presented here; for a state-of-the-art review through 1980 see Ref. 4 and for developments since 1980 see Refs. 5-7.

The first issue deals with the impact of blade rotation in turbulence modeling. Turbulence is typically modeled on the assumption that it is uniform over the rotor disk. This means that turbulence as experienced at the hub center is a representative sample of the entire disk and that the conventional body-fixed description of turbulence is satisfactory. According to this assumption, as is done for fixed-wing aircraft, the turbulence excitation at a blade station can be directly represented by models such as due to Dryden and von Karman. In sharp contrast to this assumption, which implies negligible rotational velocity effects, extensive investigations of wind turbines have shown dominant rotational velocity effects on turbulence characteristics and wind turbine blade response (Ref. 8). To present the role of rotational velocity effects in proper perspective it is expedient to study Fig. 1 (Ref. 9), which refers to an experimental and analytical investigation of a blade station of a

horizontal axis wind-turbine. It includes the predicted spectral density function of the fore-to-aft or longitudinal turbulence velocity according to the widely used von Karman turbulence model. This fore-to-aft component being perpendicular to the wind turbine plane is the most dominant component, as is the axial or vertical component for rotorcraft. Its auto-power spectral density or APSD is the Fourier transform of the auto-covariance function of the longitudinal turbulence velocity at one blade station. To capture the rotational velocity effects the data base was generated from the sampling of measurements along a circular array of points which represent the instantaneous loci of this station. The monotonically decaying behavior is exhibited by the conventional body-fixed description which fails to capture the two basic features of data: transfer of energy from essentially low-frequency region (< 1P, P: rotational speed) to the higher-than-1P region and occurrence of peaks at 1P, 2P, etc. By comparison the blade-fixed sampling description dramatically improves the correlation. The correlation also shows that the assumptions of isotropic, homogeneous and momentarily-frozen wave fields are fairly valid at low altitudes. This overall validity of these assumptions is indeed remarkable, given the complexities at low-altitude such as earth's boundary layer, closeness to obstacles and low values of turbulence scale length. Although for rotorcraft no test data on gust response exist, analytical investigations show that for conventional helicopters (advance ratios $\mu<0.4$) operating at altitudes of 1000 ft or below (turbulence scale L < 12 x rotor radius R) the widely used approximation of neglecting rotational velocity effects is not satisfactory (Refs. 9-10).

The second issue deals with spatial distribution of turbulence velocities over the rotor disk. In the past, the problem of turbulence effects on flight mechanics and vibrations was almost exclusively treated on the basis of point approximation. It is assumed that the entire rotor disk experiences a spatially uniform turbulence velocity identical to that at the rotor center so that each blade station sees the same turbulence velocity at a given time. In other words, the difference between the turbulence velocity experienced by the blade station and that experienced by the hub center is ignored. Outside the earth's boundary layer, where the turbulence scale is 600 ft or more as compared to the disk diameter of 70 ft or so, this point approximation of a small scale-vehicle encountering a large-scale turbulence is valid (Ref. 9). Within the earth's boundary layer and dependent on surface structure -- trees, buildings, bridges - the turbulence scale has values that are comparable to the rotor diameter, so that the assumption of large-scale turbulence or of a uniform turbulence velocity over the rotor disk is not a good approximation.

The third issue deals with the need for developing a turbulence simulation method that is suitable for rotorcraft applications. In fixed-wing turbulence studies, it is customary

to use transfer function models of the aircraft and combine them with appropriate turbulence spectral models for predicting aircraft turbulence response statistics. The practical utility of such an analysis is due to the facts that the aircraft is treated as a linear system with time-invariant coefficients and the turbulence is well approximated as a stationary random process. Indeed, the turbulence excitation is stationary even with inclusion of spatial distribution effects (Ref. 11) and it is a routine exercise to design shaping filters; moreover the aircraft response is also stationary and established methodology exists for its simulation. However, a straightforward application of this methodology to rotary wing turbulence is not possible. Due to combined translational and rotational velocities, each blade element traverses through a turbulence field at a different rate and samples turbulence velocities differently; hence, the simulation methods commonly used for fixed-wing turbulence are not valid for rotary-wing turbulence analysis. A rotary-wing vehicle has large periodic variations of its aerodynamic parameters and its response to turbulence is due to integrated aerodynamic loads from various blade elements. Therefore turbulence excitation and rotorcraft response to turbulence are both cyclostationary. References 12 and 13 consider turbulence simulation for rotorcraft applications based on shaping-filter and related approaches. Reference 14 considers generating sample functions of stationary turbulence on horizontal axis wind turbines. However, the simulation methods developed in Refs. 12 to 14 cannot be directly applied to the case of cyclostationary turbulence as seen by a translating and rotating blade. To reiterate, this cyclostationarity of turbulence and rotorcraft response requires a new approach to turbulence simulation methodology.

In summary, there is a need for developing atmospheric turbulence models that include effects of blade rotational velocity and spatial distribution of turbulence over the rotor disk. Also, there is a need for developing a simulation method for generating sample functions of cyclostationary turbulence.

2. OBJECTIVES

The objectives of the research are:

1. Formulate a mathematical model that describes qualitatively and quantitatively the statistics (e.g., covariance and instantaneous spectral density matrices) of atmospheric turbulence with reference to rotor blade in forward flight;
2. Develop a method for generating sample functions of turbulence for inclusion in vehicle simulation programs;
3. Develop approximations and simplifications to the turbulence simulation method towards real time implementation; and
4. Investigate the effects of turbulence on isolated blade flap-response statistics of covariance, frequency-time spectrum and average threshold-crossing rates.

3. TURBULENCE MODELING

The helicopter rotor disk experiences a complex three-dimensional turbulence. The treatment here is based on the von Karman theory of isotropic and homogeneous turbulence and on the Taylor hypothesis of momentarily frozen turbulence field (Refs. 4, 10). Extensive experimental data with respect to airplanes (Ref. 11) and wind turbines (e.g., Ref. 8) show that the von Karman theory and the Taylor hypothesis are reasonably valid. They also show that turbulence is approximately Gaussian as well. With respect to rotorcraft, similar experimental data are not available. However, following earlier studies, (e.g., Refs. 3-7 and 9-10) it is assumed that the rotor disk experiences essentially free atmospheric turbulence with negligible influence of self induced turbulence and that the vertical turbulence velocity is the most dominant component compared to the turbulence velocity components in the fore-to-aft and lateral directions. It is emphasized that the vertical turbulence is treated in a three-dimensional gust field by accounting for variations of blade-station coordinates in the fore-to-aft, lateral and vertical directions. However, for illustration the results are for level-flight conditions, when the turbulence field is two-dimensional.

All the information necessary to develop the dynamic equations describing the atmospheric turbulence velocity field experienced by a blade element is contained in the atmospheric turbulence velocity correlation matrix (Ref. 10). As shown schematically in Fig. 2 (sketches 1 and 2), subscripts 1, 2 and 3, respectively, refer to mean wind, lateral and vertical directions. For homogeneous and isotropic turbulence, the covariance matrix in one frame of reference can easily be transformed into another frame (Refs. 10, 15). For algebraic simplicity, the mean tail wind direction coincides with the flight or longitudinal direction in the present formulation.

As sketched in Fig. 2, A(t) and B(t) are the instantaneous temporal or azimuthal locations of two stations, and $A(t_1)B'(t_2)$ or ξ_{AB}, is the projection of $A(t_1)B(t_2)$ on the line in the mean wind direction from $A(t_1)$. For isotropic turbulence, the correlation function for lateral turbulence velocity u_2 is identical to that of the vertical turbulence velocity u_3. From the von Karman theory, the fundamental longitudinal correlation function f and the fundamental transverse or lateral correlation function g are

$$f_{u_1 u_1}(\xi_{AB'}, t_1, t_2) = E[u_1^A(t_1) u_1^{B'}(t_2)] \tag{1}$$

$$g_{u_2u_2}(\xi_{AB}, t_1, t_2) = E[u_2^A(t_1)u_2^{B'}(t_2)] = E[u_3^A(t_1)u_3^{B'}(t_2)] \tag{2}$$

Several models such as due to von Karman, Dryden, Rosenbrock, etc. exist in the literature (Ref. 9, 11, 16) for the fundamental longitudinal and lateral correlation functions, f and g. For example, as per von Karman model, the expressions for the fundamental longitudinal and lateral correlation functions are given by (Ref. 16)

$$f(\xi) = \frac{2^{2/3}}{\Gamma(1/3)}\left(\frac{\xi}{1.38L}\right)^{1/3} K_{1/3}\left(\frac{\xi}{1.38L}\right) \tag{3}$$

$$g(\xi) = \frac{2}{\Gamma(1/3)}\left[\frac{\xi}{2.68L}\right]^{1/3}\left[K_{1/3}(\frac{\xi}{1.34L}) - \frac{\xi}{2.68L}K_{2/3}(\frac{\xi}{1.34L})\right] \tag{4}$$

where L is scale length of the longitudinal turbulence and $K_{1/3}$ and $K_{2/3}$ are modified Bessel functions of the second kind of fractional order 1/3 and 2/3, respectively.

The distance metric ξ_{AB} (sketch 2, Fig. 2) discussed next represents the spatial separation relative to the mean wind during the lapsed time t_2-t_1. Theoretically, the nine elements of the covariance matrix between the three velocity components at $A(t_1)$ and at $B(t_2)$ are given by

$$R_{u_iu_j}(\xi_{AB}, t_1, t_2) = \frac{(f-g)\xi_i\xi_j}{|\xi|^2} + g\delta_{ij} \qquad i,j = 1,2,3 \tag{5}$$

In the above equation ξ_i represents spatial separation between A and B in the i-th direction. Thus, the problem boils down to evaluating the correlation distance or spatial separation ξ_{AB}. For example, the cross-correlation function between $u_1^A(t_1)$ and $u_2^B(t_2)$ is

$$E\left[u_1^A(t_1)u_2^B(t_2)\right] = \sigma^2\left[\frac{f(\xi_{AB}) - g(\xi_{AB})}{\xi_{AB}^2}\xi_{AB}\cdot\xi_{BB}\cdot\right] \tag{6}$$

It is clear from Eq. (6) that for level flight conditions, the velocity pairs $[u_2^A(t_1), u_3^B(t_2)]$, $[u_2^B(t_1), u_3^A(t_2)]$, $[u_1^A(t_1), u_3^B(t_2)]$ and $[u_1^B(t_1), u_3^A(t_2)]$ are not correlated.

$$E\left[u_1^A(t_1)u_3^B(t_2)\right] = E\left[u_3^A(t_1)u_1^B(t_2)\right] = E\left[u_3^A(t_1)u_2^B(t_2)\right]$$
$$= E\left[u_2^A(t_1)u_3^B(t_2)\right] = 0 \tag{7}$$

In order to understand the impact of blade rotational velocity on turbulence modeling, the case of a helicopter flying straight and level, directly into the mean head wind, is considered; see Sketch 3 of Fig. 2. Let V_{ac} and V_{mw} represent ground speeds of the rotorcraft and mean head wind , respectively. Airspeed $V=V_{ac}+V_{mw}$. The (X_H, Y_H, Z_H) and (X_B, Y_B, Z_B) systems are the conventional body-fixed and blade-fixed frames, respectively, in which the Z axis, directed downward, is the plunge direction and represents both the nonrotating vertical axis Z_H of the body-fixed system as well as the rotating shaft axis Z_B of the blade-fixed system. Both systems are right-handed; while X_H axis represents the flight direction, also referred to as the longitudinal or aft-to-fore direction, the X_B axis along the blade span represents the radial direction. For blade station A at $\xi_A R$ distance from the center ($o \le \xi_A \le 1$), the velocity components relative to the atmosphere, expressed in inertial or ground-fixed coordinates, are

$$\frac{dX}{dt} = V + \xi_A \Omega R \sin \Omega t$$
$$\frac{dY}{dt} = \xi_A \Omega R \cos \Omega t \tag{8}$$

The distance metric is the vector between two points on the lifting surfaces at two points in time in the atmospheric frame. Its magnitude is (see sketch 2 in Fig. 2)

$$|\xi| = [\{X^B(t_2) - X^A(t_1)\}^2 + \{Y^B(t_2) - Y^A(t_1)\}^2]^{1/2} \tag{9}$$

which is also referred to as the correlation distance. It is convenient to use the following dimensionless time and velocity units:

$$\bar{t}_1 = \Omega t_1, \qquad \bar{t}_2 = \Omega t_2 \tag{10}$$

$$\frac{V}{\Omega R(L/2R)} = \frac{\mu}{(L/2R)} = \frac{2\mu}{(L/R)} = a \tag{11}$$

where μ is the advance ratio. The dimensionless magnitude of the distance metric ξ_{AB} reduces to

$$\xi_{AB}(\bar{t}_1,\bar{t}_2) = \xi = \frac{L}{2}\{a^2\tau^2 + 16R_L^2\xi_A\xi_B\sin^2\tau/2 + 4aR_L(\xi_A+\xi_B)\tau\sin t\sin\tau/2 + 4R_L^2(\xi_A-\xi_B)^2 + 4aR_L(\xi_A-\xi_B)\tau\cos t\cos\tau/2\}^{1/2} \quad (12)$$

where R_L=R/L, t is the average time $(\bar{t}_1+\bar{t}_2)/2$ and τ is the lapsed time $\bar{t}_2-\bar{t}_1$. As is evident from the context and for simplicity of notation, t represents both the physical time, as in Eq. (9) and the dimensionless average time, as in Eq. (12). Also, it is observed from Eq. (12) that

$$\xi_{AB}(\bar{t}_1,\bar{t}_2) = \xi_{AB}(\bar{t}_1+2m\pi,\bar{t}_2+2n\pi) \quad (13)$$

for integer m=n only.

Under non-level flight conditions, Eq. (9) is generalized to

$$|\xi| = [\{X^B(t_2)-X^A(t_1)\}^2 + \{Y^B(t_2)-Y^A(t_1)\}^2 + \{Z^B(t_2)-Z^A(t_1)\}^2]^{1/2} \quad (14)$$

The expressions of dX/dt, dY/dt and dZ/dt would depend upon several flight mechanics details such as flight path angle, shaft tilt etc., and the expression for ξ_{AB} in closed form, as in Eq. (12), is not possible. Moreover, in contrast to Eq. (7), $E[u_1^A(t_1)u_3^B(t_2)]$, $E[u_3^A(t_1)u_1^B(t_2)]$, $E[u_2^A(t_1)u_3^B(t_2)]$, $E[u_3^A(t_1)u_2^B(t_2)]$ are not necessarily equal to 0. Moreover, Eq. (12) shows that the rotational velocity effects should decrease with increasing advance ratio. When rotational velocity effects are neglected, the magnitude of the distance metric simplifies to

$$|\xi| = \frac{L|a\tau|}{2} \quad (15)$$

Now, considering only the dominant vertical turbulence component that is nearly normal to the rotor plane and for level flight condition, the correlation of vertical component of turbulence velocity is given by

$$R_{u_3u_3}(t_1,t_2) = R_w(t_1,t_2) = \sigma^2 g(\xi_{AB}) \quad (16)$$

Correlation function between vertical turbulence velocities $w^A(t_1)$ and $w^B(t_2)$ can be obtained by substituting the expression for distance metric of Eq. (12) into Eq. (16). It is seen from Eqs. (12-13) that

$$R_w(\bar{t}_1 + 2m\pi, \bar{t}_2 + 2n\pi) = R_w(\bar{t}_1, \bar{t}_2) \qquad \text{for } m = n \text{ only} \tag{17}$$

or, equivalently,

$$R_w(t + 2m\pi, \tau) = R_w(t, \tau) \qquad \text{for } m = 0, 1, 2, \ldots \tag{18}$$

Equation (17) shows that the blade-sampled turbulence belongs to a (wide sense) cyclostationary process (Refs. 17-20). However, the process is not mean square periodic since Eq. (18) does not hold for $m \neq n$ (Ref. 17). From Eq. (17), the process is also not (weakly) stationary since $R_w(t_1,t_2)$ is not a function of t_2-t_1 only (Ref. 17). Moreover, Eq. (17) or (18) shows that the correlation, though not invariant to arbitrary shifts of t_2-t_1 as in a stationary process, is invariant to shifts of integer multiples of 2π. This nearness to stationarity is better explored by means of frequency-time spectrum or the Wigner distribution (Refs. 21, 22).

The frequency-time spectrum $S_w(f,t)$ is obtained by taking the Fourier transform of $R_w(t,\tau)$ with respect to τ (Ref. 21),

$$S_w(f,t) = \int_{-\infty}^{\infty} R_w(t,\tau) e^{-i2\pi f\tau} d\tau \tag{19}$$

It is possible to obtain a closed-form expression for the frequency-time spectrum for the case of $\xi_A = \xi_B$ and in level flight using Rosenbrock model for the fundamental correlation functions, f and g, as in Refs. 9 and 23. The closed-form solution permits qualitative and parametric investigation of rotational velocity effects on turbulence modeling. Thus with the Rosenbrock model given by

$$R_w(\xi) = \sigma^2 e^{-4\xi^2/L^2} \tag{20}$$

substituting the distance metric expression from Eq. (12) with $\xi_A = \xi_B = 0.7$ in Eq. (20) results in

$$R_w(t,\tau) = \exp\left\{-\left(a^2\tau^2 + 4c^2 \sin^2\frac{\tau}{2} + 4ac\tau \sin t \sin\frac{\tau}{2}\right)\right\} \tag{21}$$

where c=1.4/(L/R). Substituting Eq. (21) in Eq. (19) and after several algebraic manipulations (for details see Refs. 9 and 23), the following expression for the frequency-time spectrum of blade sampled vertical turbulence is obtained:

$$S_w(f,t) = \frac{1}{\pi}\sum_{s=0}^{\infty}\sum_{q=0}^{\infty}\sum_{p=-[(q/2)+s]}^{p=[(q/2)+s]} \frac{(-1)^{q+s}(q+2s)!B^{2s}C^{q}}{2^{q+2s}q!s![(q/2)+s+p]![(q/2)+s-p]!}$$

$$x\left\{(-1)^{p}T_1(q)\frac{\Gamma[(q+1)/2]}{2A^{q+1}}\phi\left(\frac{q+1}{2},\frac{1}{2},\frac{-(f+p)^2}{4A^2}\right)\right.$$

$$+(-1)^{\frac{2p+1}{2}}T_2(q)\frac{(f+p)\exp[-(f+p)^2/4A^2]}{2A^{q+2}}$$

$$\left.x\Gamma\left(\frac{q+1}{2}\right)\phi\left(\frac{1-q}{2},\frac{3}{2},\frac{(f+p)^2}{4A^2}\right)\right\} \qquad (22)$$

where $T_1(q)=1$, $T_2(q)=0$, for q=0,2,4,6,.... even
$T_1(q)=1$, $T_2(q)=1$, for q=1,3,5,7,.... odd
ϕ is degenerate hypergeometric function.

Equation (22) is instructive in that the variation of $S_w(f,t)$ for instantaneous azimuth locations has preferred locations at 1P/2, 1P, 3P/2, etc. Figure 3 shows perspectives of the correlation and frequency-time spectral density for the Rosenbrock model for μ=0.05 and L/R=4. Figure 3 illustrates rotational velocity effects on turbulence modeling as turbulence frequency-time spectral concentration within preferred frequency bands centered on 1P/2, 1P, 3P/2, etc. By contrast, the conventional body-fixed turbulence modeling suppresses such peaks with rapid attenuation of such peaks with increasing frequency.

Using a mathematical model of an isolated rigid root-restrained blade, the impact of turbulence velocity effects on turbulence modeling and flap response statistics is investigated in Ref. 9. Based on the numerical results for various values of advance ratio and turbulence scale length, it is shown therein that the response statistics comprising frequency-time spectra, the conventional correlations, and the average threshold upcrossing rates are significantly affected by the rotational velocity effects and these effects decrease with increasing advance ratio and turbulence scale length.

5. ROTORCRAFT TURBULENCE SIMULATION

For convenience of illustration, a helicopter in level flight is considered. The most general representation comprises all the three velocity components in a three-dimensional turbulence field -- vertical, lateral (side-to-side) and longitudinal (fore-to-aft) velocities - the distance metric for each component accounts for spatial changes in all the three directions. First, consider only the vertical turbulence velocities felt by a rotor in level flight, heading into the mean wind direction. The correlation function, R_{33}, for this case is given by Eq. (16) with the distance metric ξ_{AB} given by Eq. (12).

For simulation purposes, it is important to consider the time lag between the hub center and a typical blade station in experiencing turbulence. Considering a simplified picture of the spatial variation of turbulence in the flight direction only (i.e., a one-dimensional distribution of turbulence), as compared to the hub, an element located at radius r and azimuthal angle ψ will experience turbulence velocities with a time lag, Δt, given by

$$\Delta t = \frac{r \cos \psi}{V} \tag{23}$$

Denoting $w_{hub}(t)$ and $w_{blade}(r,t)$ as sample functions of turbulence velocity felt at the hub center and the blade station, respectively, $w_{hub}(t)$ and $w_{blade}(r,t)$ are related through the expression for the time lag of Eq. (23)(Ref. 24):

$$w_{blade}(r,t) = w_{hub}(t - \frac{r \cos\psi}{V}) \tag{24}$$

The term $r\cos\psi/V$ in Eq. (24) accounts for the effects of both rotational velocity and the spatial distribution of turbulence. From Eq. (24), it is seen that the time lag increases with increasing radial distance and decreasing airspeed. Thus, rotational velocity effects will be dominant at the blade tip for low airspeeds.

Using Shinozuka's algorithm (Ref. 25), $w_{hub}(t)$ can be expressed in terms of a series of cosine fucntions as

$$w_{hub}(t) = 2 \sum_{i=1}^{N} \sqrt{S_{33}(\omega_i)\Delta\omega} \cos(\omega_i t + \Phi_i) \tag{25}$$

where $S_{33}(\omega_i)$ is the value of the two-sided, power spectral density (corresponding to the correlation function, R_{33}) of the stationary turbulence process at the *temporal* frequency ω_i and Φ_i is random phase with uniform probability density distribution between 0 and 2π. The discrete frequency ω_i is obtained by dividing the frequency band of interest of the power spectral density curve into almost equal subdivisions:

$$\omega_i = (2i-1)\Delta\omega/2, \qquad i = 1,2,...,N \tag{26}$$

Combining Eqs. (24) and Eq. (25) results in

$$w_{blade}(r,t) = 2\sum_{i=1}^{N} \sqrt{S_{33}(\omega_i)\Delta\omega}\cos[\omega_i(t - \frac{r\cos\psi}{V}) + \Phi_i)] \tag{27}$$

Equation (27) can be rewritten in terms of positive spatial frequencies ω_k and $\Delta\omega$ as

$$w_{blade}(r,t) = 2\sum_{k=1}^{N} \sqrt{S_{33}(\omega_k)\Delta\omega}\cos[\omega_k(Vt - r\cos\psi) + \Phi_k)] \tag{28}$$

Thus, Eq. (28) gives an expression for the sample function for the vertical turbulence as seen by a rotating blade element.

Thus far, since the frozen field of vertical turbulence velocity is approximated in terms of one-dimensional waves, the turbulence velocity at a point located at (x,y,z) in the atmospheric frame is written as a function of x alone. In reality, the correlation of vertical turbulence velocities is a function of all the three components of spatial separation and the corresponding spectral density is a function of three spatial frequencies, ω, ν, κ; a three-dimensional spectrum.

The simulation method described above can be extended to the cases of two- and three- dimensional distributions of vertical turbulence. For the case of two-dimensional distribution of vertical turbulence the expression for w(r,t), including rotational velocity effects, reduces to (Ref. 24)

$$w(r,t) = 2\sum_{j=1}^{N_1}\sum_{k=-N_2}^{N_2} \sqrt{S_{33}(\omega_j,\nu_k)\Delta\omega\Delta\nu}\cos(\omega_j(Vt - r\cos\psi) + \nu_k(r\sin\psi) + \Phi_{j,k}) \tag{29}$$

where

$$\omega_j = (2j-1)\Delta\omega/2$$
$$\nu_k = (2k-1)\Delta\nu/2$$

The expression for w(r,t) for the case of three-dimensional spectrum is given by (Ref. 24)

$$w(r,t) = 2\sum_{i=1}^{N_1}\sum_{j=-N_2}^{N_2}\sum_{k=-N_3}^{N_3}\sqrt{S_{33}(\omega_i,\nu_j,\kappa_k)\Delta\omega\Delta\nu\Delta\kappa}\,\cos\left(\omega_j x + \nu_j y + \kappa_k z + \Phi_{i,j,k}\right) \quad (30)$$

where x, y and z represent the three components of the location of the blade element measured in the atmosphere-axis system and ω, ν, κ are the corresponding spatial frequencies.

Using numerical results for the two-dimensional case, it is shown in Ref. 24 that sample functions generated using the simulation method described above will contain the correct second order statistics as seen by a rotating and translating blade element. Reference 26 presents a generalization of the above simulation method to include all three components of turbulence velocities using the turbulence spectral matrix.

6. APPROXIMATIONS TO TURBULENCE SIMULATION

The turbulence simulation method presented in the previous section in its present form is not suitable for real-time implementation as it involves for the three-dimensional case triple summation of terms over several frequency values in the expression for turbulence velocities. Also, for real-time implementation, the type of turbulence distribution, i.e, 1-D, 2-D or 3-D, as well as the number of blade elements and the number of azimuthal locations at which turbulence velocities need to be computed become important.

Reference 27 addresses the issue of minimum number of blade stations at which turbulence velocities need to be computed for adequate representation of turbulence effects on blade response. Using a mathematical model representation of an articulated rigid root-restrained blade, flap response statistics are computed and compared for different number of blade stations. Also, comparisons are made between response results with one-dimensional and two-dimensional turbulence distributions. Figures 4 and 5 describe the mean square flapping response and zero exceedance statistics (average number of response up-crossings per unit time) of flapping response, respectively. Four curves are shown in these figures. The line labeled as 'body fixed' represents results for the case wherein turbulence velocity computed at the hub center is used for the entire rotor and the turbulence simulation involves single summation of sinusoids at one blade station. The other three lines represent results with blade-fixed sampling. The line labeled as 'One-Dimensional' represents results for the case wherein turbulence velocity is computed at several blade stations (eight in this study) but with the assumption of one-dimensional distribution (see Eq. (28)). The turbulence simulation for this case involves single summation of sinusoids at several blade stations. The line labeled as '75% Approximation' represents results for the case wherein turbulence velocity computed at the 75% radial station with a two-dimensional distribution is used for the entire blade and the simulation method involves double summation of sinusoids (see Eq. (29)) at one blade station. The line labeled as 'Two-Dimensional' represents results for the case wherein turbulence velocity is computed at several stations (eight stations in this study) with a two-dimensional distribution (see Eq. (29)). The two-dimensional case involves double summation of sinusoids at several blade stations and it is the most accurate of the four cases. It is emphasized that the one- and two-dimensional results include the effect of cross-correlation of turbulence velocities on various elements of the blade. It is seen from Figs. 3 and 4 that the 'body-fixed' and 'one-dimensional' cases result in very inaccurate predictions of blade response. Surprisingly, the

'75% approximation' results are very close to the 'two-dimensional' case. Based on these results, Ref. 27 concludes that a two-dimensional distribution of turbulence is required in order to capture the effects of turbulence on blade response. Also, it is adequate to use the three-quarter radial station as a representative station for obtaining a reasonably accurate prediction of turbulence effects on blade response.

The number of terms involved in the summation for simulation of sample functions of two-dimensional vertical turbulence is considered next. The expression for sample function of vertical turbulence velocity given by Eq. (29) involves summation of terms over spatial frequencies ω and ν. Transforming Eq. (29) to polar coordinates using

$$\begin{aligned} \omega &= \Omega \cos\theta \\ \nu &= \Omega \sin\theta \end{aligned} \tag{31}$$

results in

$$w(r,t) = 2 \sum_{l=1}^{N_3} \sum_{j=1}^{N_4} \sqrt{2S_{33}(\Omega_i, \theta_j)\Omega_i \Delta\Omega\Delta\theta}\, \cos(\Omega_i \cos\theta_j (Vt - r\cos\psi) + \Omega_i \sin\theta_j (r\sin\psi) + \Phi_{i,j}) \tag{32}$$

In Eq. (32), the summation limits for the transformed variables Ω and θ are as follows:

Ω: 0 to Ω_{max}
θ: 0 to $\pi/2$

Reference 26 uses 110 values for ω and ν each (i.e., N_1=110, N_2=110) in Eq. (29) for accurate representation of rotational velocity effects. However, Ref. 28 shows that if one uses Eq. (32) instead of Eq. (29) , then the number of terms required in simulation for accurate representation of rotational sampling effects are significantly reduced.

Even with the use of polar coordinate representation (see Eq. (32)) in turbulence simulation, the computational effort involved may still be high for implementation of the simulation method in a real time simulator. For this reason, the feasibility of approximating the double summation in the expression for 2-D turbulence sample function by an equivalent single summation is investigated in Ref. 28. Reference 25 provides motivation for such an approximation wherein it is shown that sample functions for a non-homogeneous random process can be simulated by using its power spectral density multiplied by a modulating function that characterizes the non-homogeneity of the process. Extending this idea to the case of blade-fixed cyclostationary turbulence, it may be possible

to arrive at a suitable modulating function which, when used in conjunction with a 1-D spectral distribution and hence, single summation of terms, approximates a 2-D spectral distribution. Reference 28 identifies such a modulating function and gives the following expression for single summation approximation to 2-D vertical turbulence sample function for a blade station located at a point (x, y) in the atmospheric frame :

$$w(x,y) = 2\sum_{i=1}^{N_1} \sqrt{f(x,y)S_{33}(\omega_i)\Delta\omega}\cos(\omega_i\xi + \Phi_i) \tag{33}$$

where $S_{33}(\omega)$ is 1-D vertical turbulence spectrum and

$$\begin{aligned} f(x,y) &= \frac{s}{p}\frac{V_p}{V} \\ s &= \sqrt{x^2 + y^2} \\ V_p &= \sqrt{(\frac{dx}{dt})^2 + (\frac{dy}{dt})^2} \\ p &= \int_0^t V_p dt \\ \xi &= s\left|\frac{ds}{dt}\right| \end{aligned} \tag{34}$$

Using numerical results it has been shown in Ref. 28 that the single summation approximation to the expression for sample functions of vertical turbulence described above results in reasonably accurate second order statistics. Also, Ref. 28 investigates development and use of parallel computing schemes for turbulence simulation and for prediction of turbulence statistics.

6. ROTATIONAL VELOCITY EFFECTS ON BODY RESPONSE

The effect of rotational sampling of turbulence on helicopter body response has been qualitatively investigated in Ref. 26. In order to carry out this investigation, the turbulence simulation method was first integrated into the UH-60A Black Hawk helicopter simulation program (Ref. 29). The vehicle was initially trimmed at an advance ratio of 0.1 and the main rotor was subjected to a two-dimensional vertical turbulence velocity distribution given by von Karman model with an intensity of 5 ft/sec and L/R of 2. The normal acceleration response results are shown in Fig. 6 for the cases of with and without rotational velocity effects. It is seen from Fig. 6 that for the case without rotational velocity effects, the normal acceleration response is essentially of low frequency. However, for the case with rotational velocity effects, the low frequency response is attenuated and it is replaced by low-amplitude high frequency response. Though not shown, the body pitch and roll rate responses exhibit similar characteristics. Based on the qualitative differences seen in body response results with and without rotational velocity effects, Ref. 26 concludes that the effect of rotational sampling on vehicle response is to attenuate the low frequency (<1P) response of the vehicle and to amplify the high frequency (≥1P) vibration.

7. CONCLUSIONS

Based on various results obtained in this study the following general conclusions are made :

1. A generalized formulation of the correlation matrix describing atmospheric turbulence that a rotating blade element encounters has been developed.

2. Using a closed-form solution of frequency-time spectrum of the dominant vertical turbulence excitation at an arbitrary blade station, it has been shown that the blade flap response statistics comprising frequency-time spectra, the conventional correlations, and the average threshold crossing rates are significantly affected when rotational velocity effects are included in turbulence modeling.

3. A simulation method suitable for rotorcraft turbulence analysis has been developed. It is shown that the simulation method is capable of generating samples of vertical turbulence velocities with correct second order statistics as seen by a rotating and translating blade element.

4. The simulation method for generation of sample functions of vertical turbulence has been generalized for arbitrary motion of a blade element and the same has been integrated into a comprehensive flight simulation program. Using representative results of vehicle response in the presence of vertical turbulence, it has been shown that the effect of rotational velocity results in a decrease of low frequency ($< 1P$) response of the body and an increase in high frequency ($\geq 1P$) vibrations.

5. Using a mathematical model of an articulated rigid root-restrained blade, flap response statistics have been computed and compared for one- and two-dimensional turbulence distributions. Using representative results for mean square flapping response and zero exceedance statistics, it has been shown that a two-dimensional distribution of turbulence is required in order to capture the effects of turbulence on blade response.

8. RECOMMENDATIONS

1. Experimental validation of the rotorcraft turbulence modeling and analysis approach developed in this study needs to be conducted.
2. An improved understanding of turbulence is needed for non-level-flight conditions of helicopters and tiltrotors such as axial flights, transition flights, landing approaches, nap-of-the-earth or NOE flights and hovering. The current formulation with blade rotational velocity effects is restricted to a two-dimensional turbulence field of level-flight conditions and considers only vertical turbulence at a helicopter blade station near the tip; it thus completely neglects cross-correlation between vertical, longitudinal and lateral turbulence velocities at different blade stations and also neglects turbulence in the longitudinal and lateral directions.
3. Several approximations to the simulation method have been studied in this work. Further work is required to investigate real-time simulation of blade-sampled turbulence.
4. The Taylor-von Karman turbulence theory provides the basis of all the turbulence work on helicopters and tiltrotors. This theory, though reasonably valid for level-flight conditions, is not valid in hovering. Its range of validity for different non-level flight conditions is seldom verified. Much research is needed to provide a means of quantifying the range of non-applicability of this theory for different flight conditions and to develop a viable turbulence theory for such flights.

REFERENCES

1. Ham, N.D., "Active Control of Gust and Interference Induced Vibration of Tilt-Rotor Aircraft," Proceedings of the American Helicopter Society Annual Forum, May 1989.

2. Chalk, C.R. and Radford, R.C., "Mission-Oriented Requirements for Updating MIL-H-8501 Calspan Proposed Structure and Rationale," NASA CR 177371, September 1985.

3. Costello, M.F., "A Theory for the Analysis of Rotorcraft Operating in Atmospheric Turbulence," Proceedings of the 46th Annual National Forum of the American Helicopter Society, Washington, D.C., May 1990, pp. 1003-1015.

4. Gaonkar, G.H., "Gust Response of Rotor and Propeller Systems," Journal of Aircraft, Vol. 18, No. 5, 1981, pp. 389-396.

5. Gaonkar, G.H., "A Perspective on Modeling Rotorcraft in Turbulence," Probabilistic Engineering Mechanics Journal, Vol. 3, No. 1, 1988, pp. 36-42.

6. Gaonkar, G.H. and Hohenemser, K.H., "An Advanced Stochastic Model for Threshold Crossing Studies of Rotor Blade Vibrations," AIAA Journal, Vol. 10, No. 8, 1972, pp. 100-1101.

7. Gaonkar, G.H. and Hohenemser, K.H., "Comparison of Two Stochastic Models for Threshold Crossing Studies of Rotor Blade Vibrations," AIAA/ASME 12th Structures, Structural Dynamics, and Materials Conference, AIAA Paper 71-389, Anaheim, CA, April 1971.

8. Kristensen, L. and Frandsen, S., "Model for Power Spectra of the Blade of a Wind Turbine Measured from the Moving Frame of Reference," Journal of Wind Engineering and Industrial Aerodynamics, Vol. 10, 1982.

9. George, V.V., Gaonkar, G.H., Prasad, J.V.R. and Schrage, D.P., "Adequacy of Modeling Turbulence and Related Effects on Helicopter Response," American Institute of Aeronautics and Astronautics Journal, Vol. 30, No. 6, June 1992, pp. 1468-1479.

10. Costello, M., Prasad, J.V.R., Schrage, D.P. and Gaonkar,G.H., "Some Issues on Modeling Atmospheric Turbulence Experienced by Helicopter Rotor Blades," Journal of the American Helicopter Society, Vol. 37, No. 2, April 1992, pp. 71-75.

11. Hoblit, F.M., Gust Loads on Aircraft: Concepts and Applications, AIAA Education Series, Washington, D.C., 1988.

12. Dahl, H.J. and Faulkner, A.J., "Helicopter Simulation in Atmospheric Turbulence," Vertica, Vol. 3, 1979, pp. 65-78.

13. Judd, M. and Newman, S.J., "An Analysis of Helicopter Rotor Response due to Gust and Turbulence," Vertica, Vol. 1, 1977, pp. 179-188.

14. Reeves, P.M., "A Non-Gaussian Turbulence Simulation," AFFDL-TR-69-67, Air Force Systems Command, Wright Patterson Airforce Base, Ohio, November 1969.
15. Hinze, J.O., Turbulence, Second Edition, McGraw-Hill Book Company, New York, 1975, Chapter 1.
16. Etkin, Bernard,: Dynamics of Atmospheric Flight, John Wiley & Sons, Inc., New York, 1972.
17. Papoulis, A., Probability, Random Variables and Stochastic Processes, McGraw-Hill, New York, 1984, Chap.9.
18. Gardner, W., Statistical Spectral Analysis, Prentice-Hall, Englewood Cliffs, NJ, 1988, Chap. 10.
19. Ogura, H., "Spectral Representation of a Periodic Nonstationary Process," IEEE Transactions on Information Theory, Vol. IT-17, No. 2, 1971, pp. 143-149.
20. Gardner, W.A., Introduction to Random Processes, McGraw-Hill, St. Louis, MO, 1990, Chap. 12.
21. Bendat, J.S. and Piersol, A.G., Random Data, Wiley, New York, 1986, Chap. 12.
22. Classen, T.A.C.M. and Mecklenbrauker, W.F.G., "The Wigner Distribution - A Tool for Time-Frequency Signal Analysis," Philips Journal of Research, Vol. 35, No. 3, 1980, pp. 217-249.
23. George, V.V., "Frequency-Time Spectral Analysis of Helicopter Turbulence and Response in Forward Flight," M.S. Thesis, Florida Atlantic University, Boca Raton, FL, Dec. 1990.
24. Riaz, J., Prasad, J.V.R., Schrage, D.P. and Gaonkar, G.H., "Atmospheric Turbulence Simulation for Rotorcraft Applications," Journal of the American Helicopter Society, Vol. 38, No. 1, January 1993, pp. 84-88.
25. Shinozuka, M. and Jan, C.-M., "Digital Simulation of Random Processes and Its Applications," Journal of Sound and Vibration, Vol. 25, No.1, 1972, pp. 111-128.
26. Riaz, J., "A Simulation Model of Atmospheric Turbulence for Rotorcraft Applications," Ph.D. Thesis, School of Aerospace Engineering, Georgia Institute of Technology, May 1992.
27. Prasad, J.V.R., Riaz, J., Gaonkar, G.H., and Dang, Y., "Parallel Implementation Aspects of a Rotorcraft Turbulence Simulation Method" Proceedings of the American Helicopter Society 49th Annual Forum, St. Louis, MO, 1993.
28. Dang, Y., Gaonkar, G.H., Prasad, J.V.R. and Zhang, H., "Parallel Computing of Helicopter Response to Turbulence Toward Real-Time Implementation," Proceedings of the American Helicopter Society 50th Annual Forum, Washington, D.C., May 11-13, 1994.

29. Howlett, J. J., UH-60A Black Hawk Engineering Simulation Program, NASA Contract NAS2-10626, December 1981.

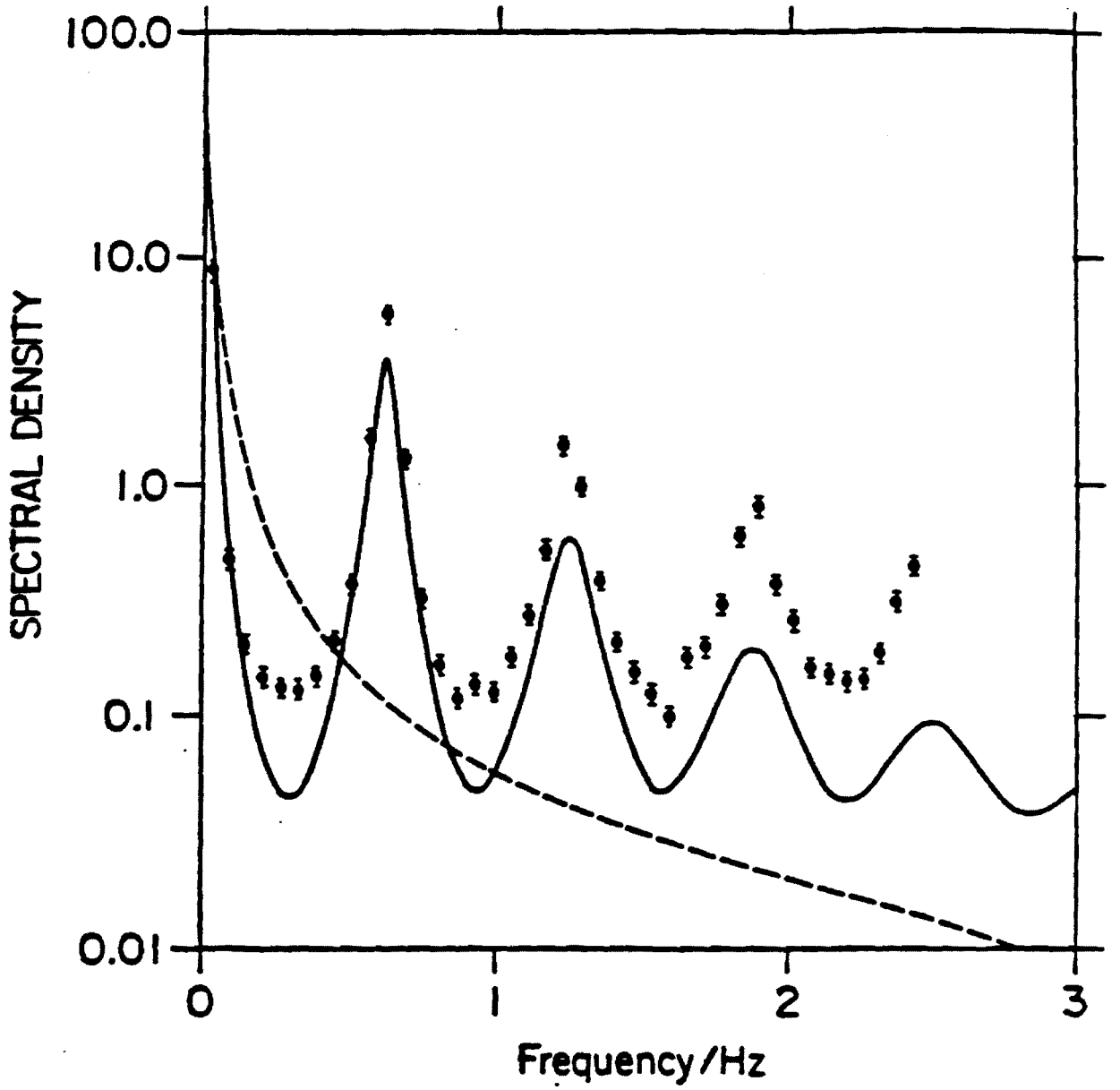

Figure 1. Autospectral densities of fore-to-aft turbulence seen by a rotating blade station and the center of the turbine disk: (1) at the blade station, blade-fixed sampling or with rotational velocity effects; (2) at the turbine disk center, body-fixed sampling or without rotational velocity effects. (Ref. 9).

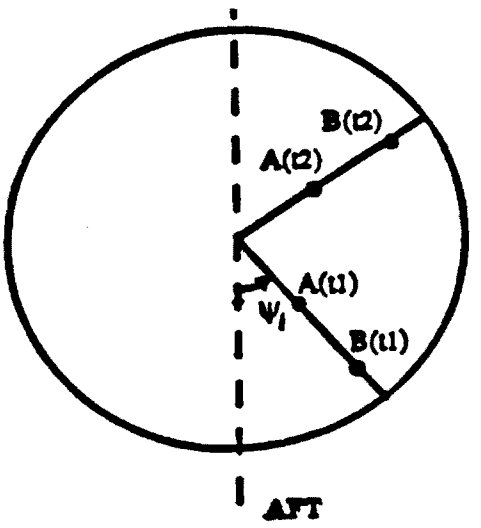

Sketch 1. Blade stations A and B at times t_1 and t_2

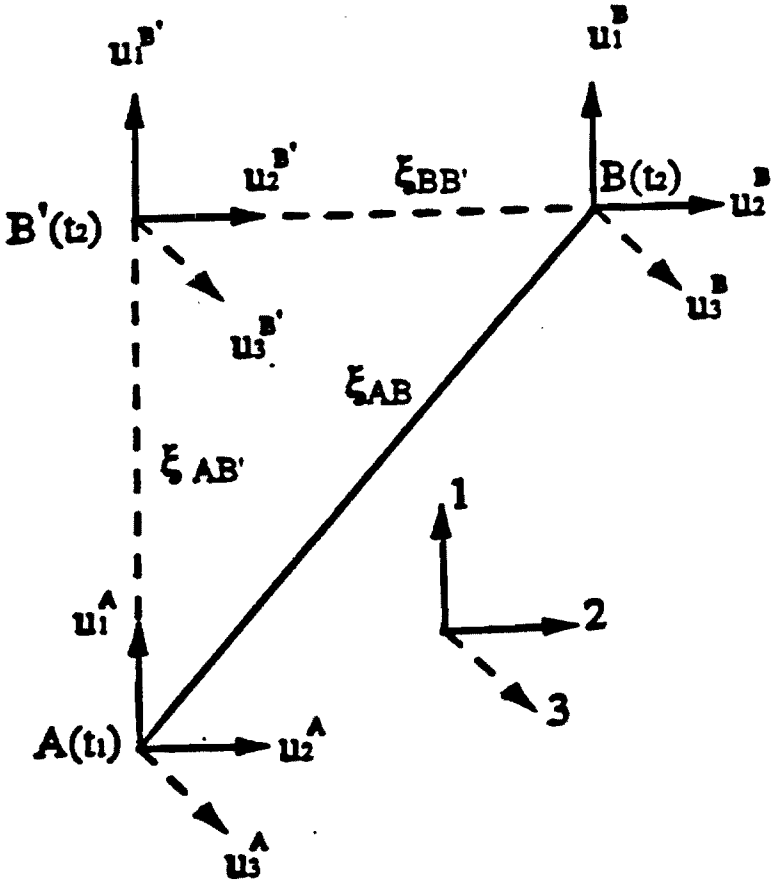

Sketch 2. Turbulence velocities at $A(t_1)$ and $B(t_2)$

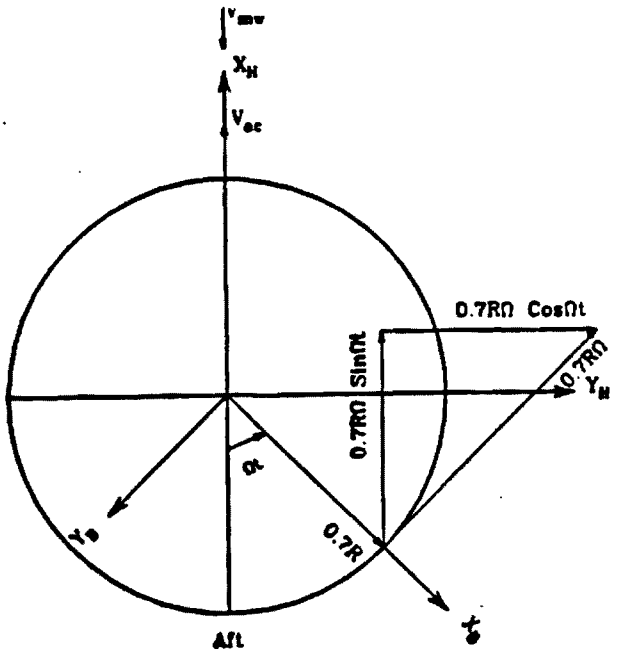

Sketch 3. Blade-fixed and body-fixed frames with head wind velocity V_{mw}

Figure 2. Schematic of distance metric ξ.

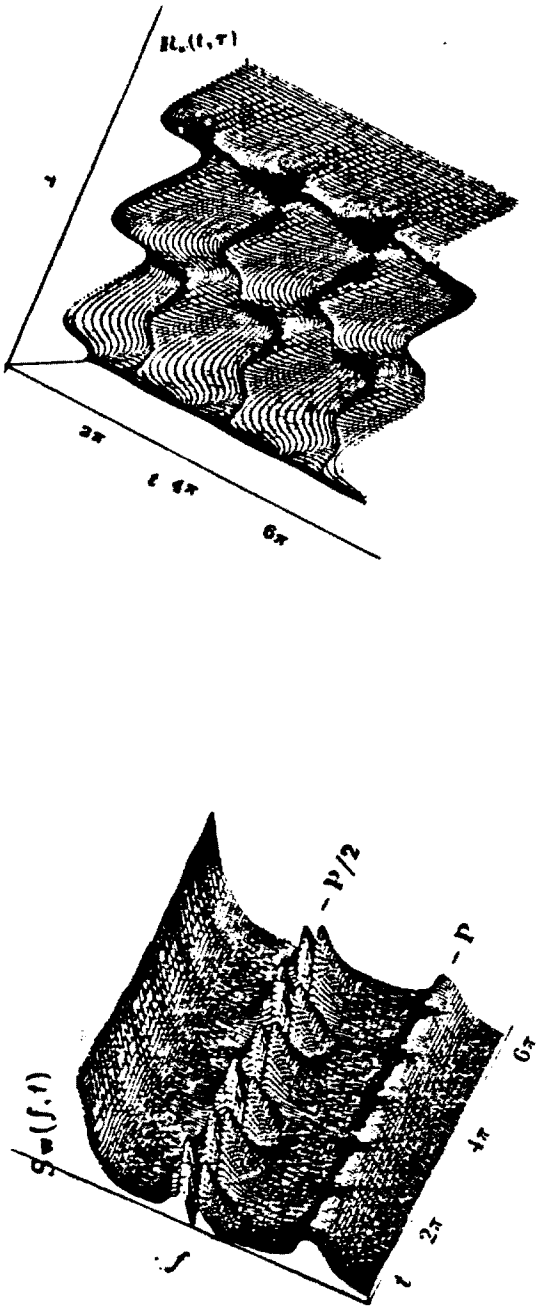

Figure 3. Perspectives of correlation and frequency-time spectrum of turbulence with rotational velocity effects (Rosenbrock model, L/R=4, μ=0.05).

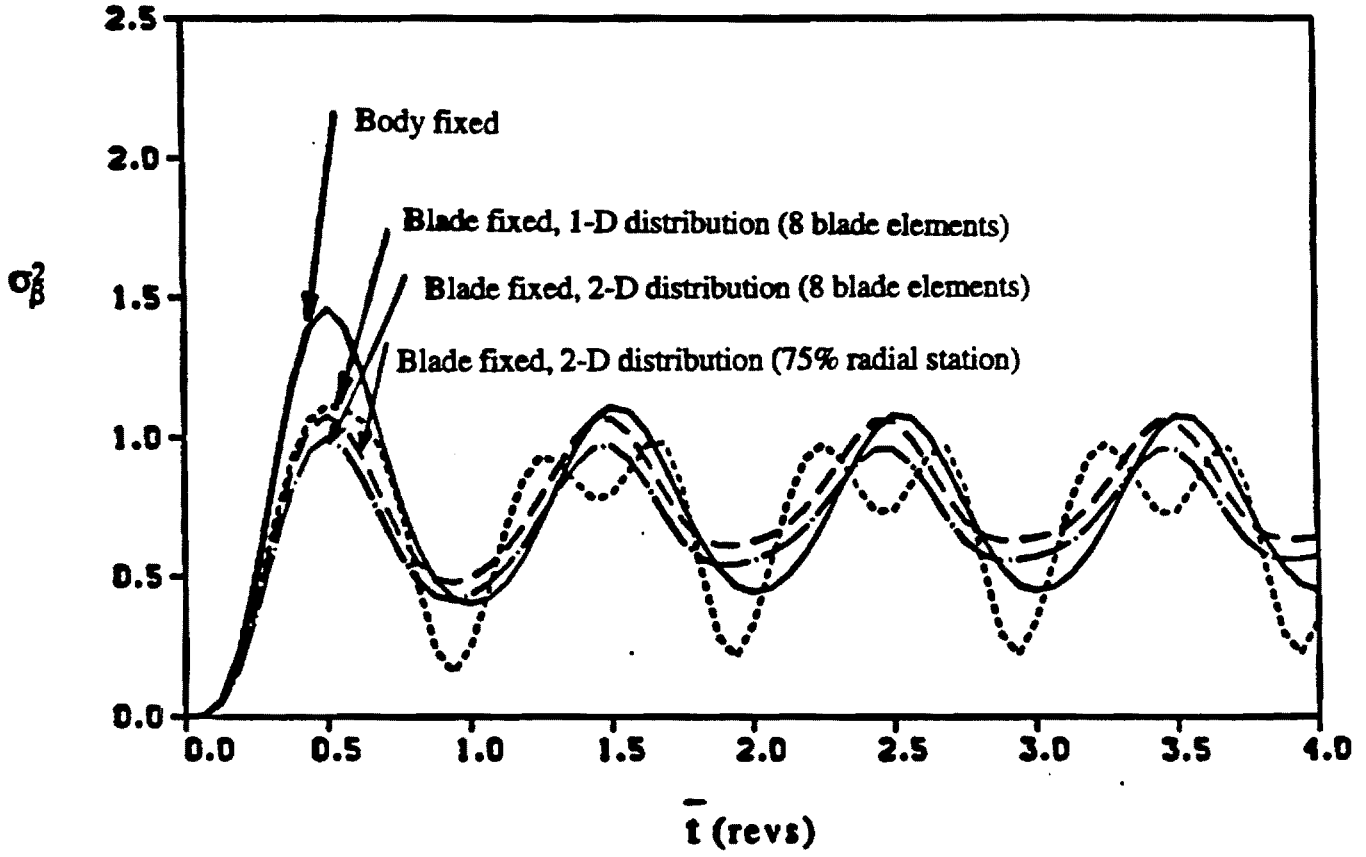

Figure 4. Mean square values of flap response (von Karman model, L/R=2, μ=0.1).

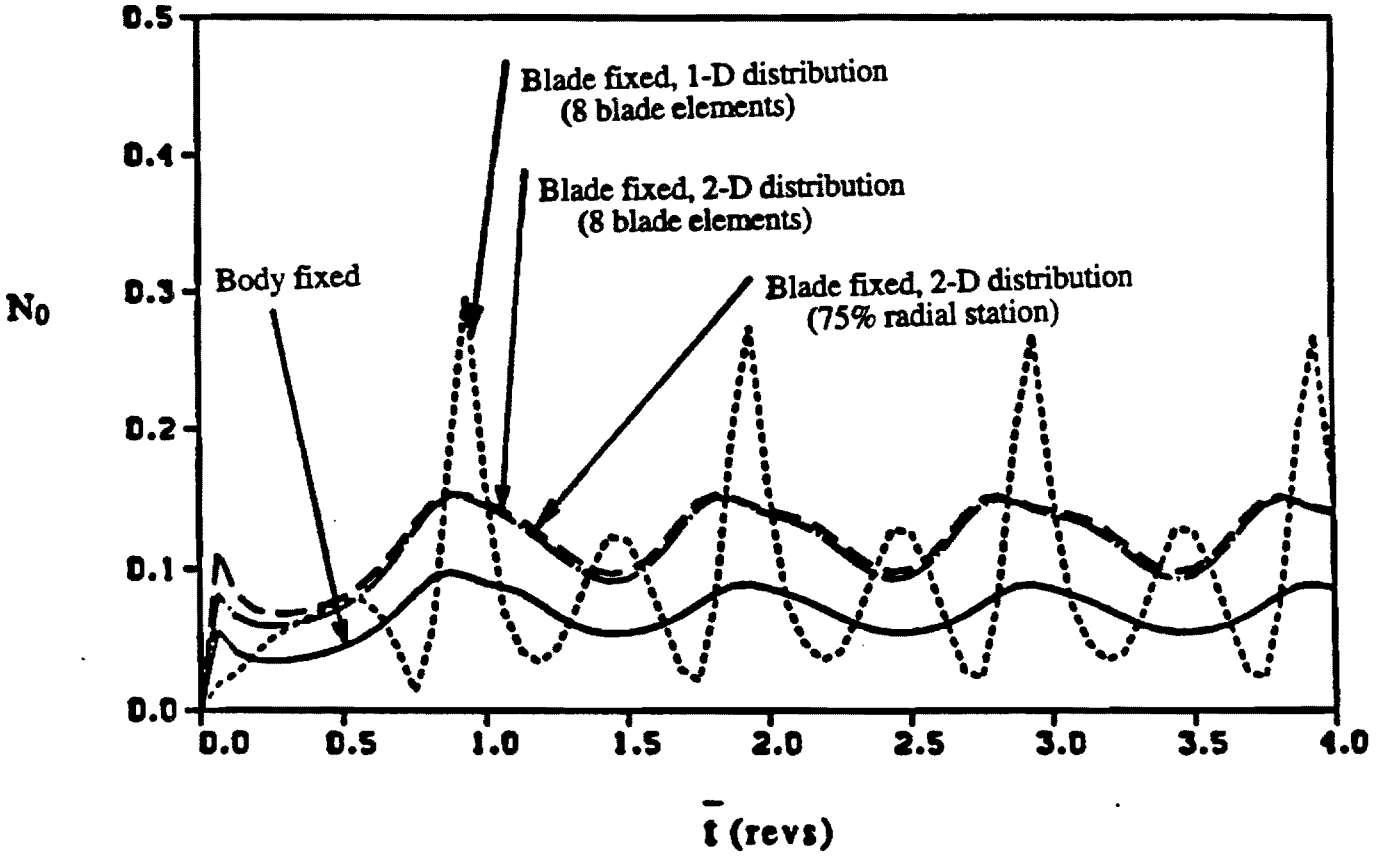

Figure 5. Zero exceedance statistics of flap response (von Karman model, L/R=2, μ=0.1).

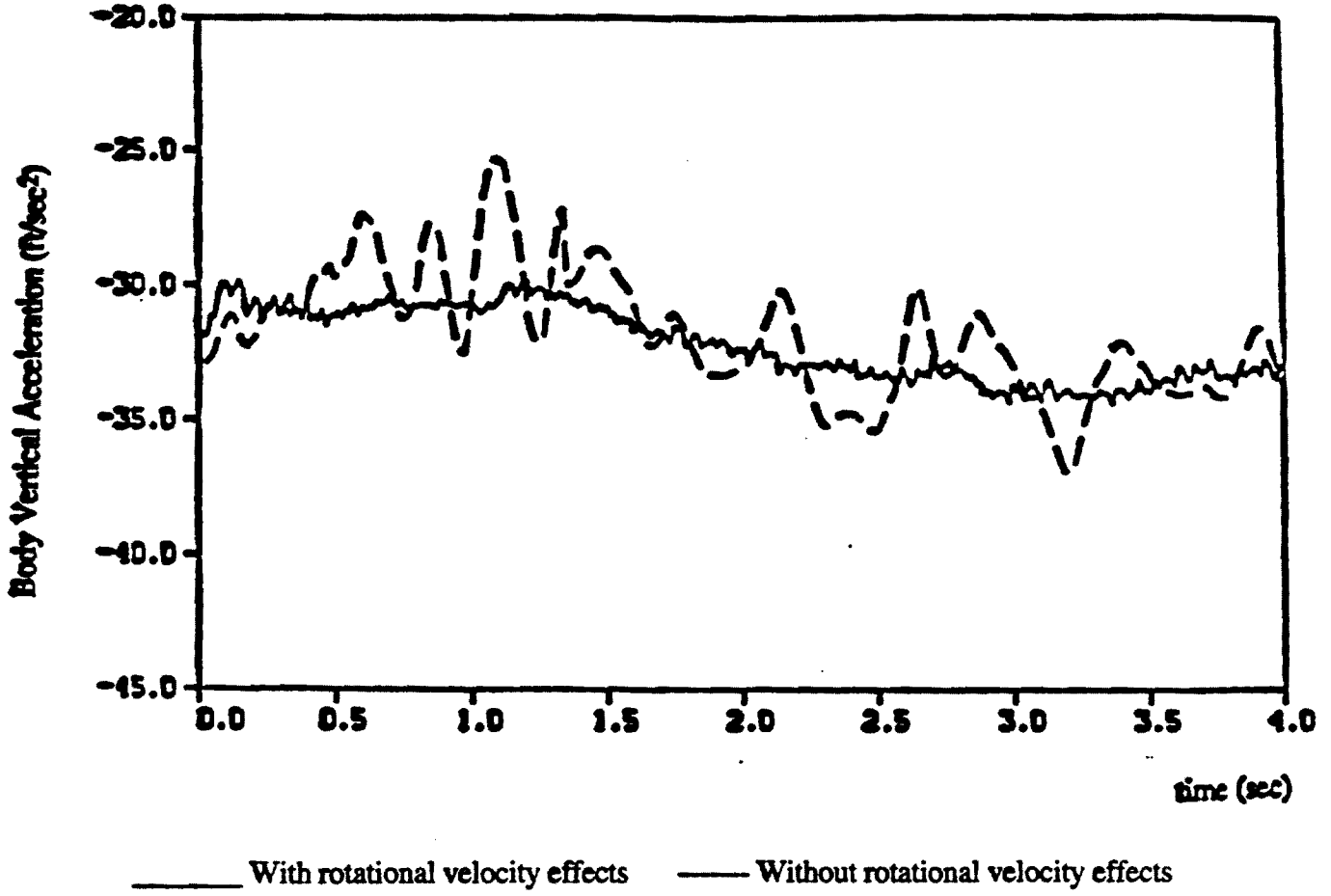

Figure 6. Sample of simulated helicopter response to two-dimensional turbulence with and without rotational velocity effects (von Karman model, L/R=2, μ=0.1).